Nanoscale mapping of wavelength-selective photovoltaic responses in H- and J-aggregates of azo dye-based solar cell films

Shashank Shekhar, Inkyoung Park, Jeongsu Kim, Myungjae Yang, Duckhyung Cho, Seunghun Hong

Journal of
Materials Chemistry A

Materials for energy and sustainability

Accepted Manuscript

This article can be cited before page numbers have been issued, to do this please use: S. Shekhar, I. Park, J. Kim, M. Yang, D. Cho and S. Hong, *J. Mater. Chem. A*, 2020, DOI: 10.1039/D0TA07328H.

ROYAL SOCIETY OF CHEMISTRY

rsc.li/materials-a

View Article Online
DOI: 10.1039/D0TA07328H

PAPER

Nanoscale Mapping of Wavelength–Selective Photovoltaic Responses in H– and J–Aggregates of Azo Dye–based Solar Cell Films

Received 27th July 2020,
Accepted 00th January 20xx

DOI: 10.1039/x0xx00000x

Shashank Shekhar,[a] Inkyoung Park,[a] Jeongsu Kim,[a] Myungjae Yang,[a] Duckhyung Cho[a] and Seunghun Hong *[a]

Nanoscale wavelength–selective photovoltaic activities in H– and J–aggregates of azo–dye–based solar cell films are mapped by a wavelength–dependent photoconductive noise microscopy. In this strategy, local conductivities and charge–traps in dye films are mapped by a conducting probe scanning on the surface while illuminating the lights with selected wavelengths. We observed the formation of localized domains exhibiting wavelength–dependent photoconductivities. The individual domains could be identified as *J*– and *H*–aggregates, which show dominant photoexcitations at wavelengths *600* and *450* nm, respectively. Notably, the short–circuit currents I_{sc} and photoconductivities $\Delta\sigma_{PC}$ of the film show power–law dependences with the trap densities under illuminated conditions (N_{T_L}) and the trap density change by illuminations (ΔN_T), respectively, like $\Delta\sigma_{PC} \propto |\Delta N_T|^{1/2}$ and $I_{sc} \propto N_{T\_L}{}^{-3/4}$ for each wavelengths illumination. These results reveal the carrier recombination process cooperated by traps which can be a major factor determining the performance of solar cells. Significantly, J–aggregates show lower trap densities than those of H–aggregates, resulting in superior solar cell characteristics of J–aggregates, such as higher I_{sc} and larger open circuit voltages. Since our method allows one to map the nanoscale photovoltaic activities of solar cell film aggregates, it can be a powerful tool for both basic researches and applications of photoelectronic devices.

1. Introduction

Dye–based solar cells can be a promising source of clean energy due to their high performances, easy–processabilities and a low cost.[1–10] Dyes' superb characteristics, such as high absorption coefficients, high luminescence efficiencies, the wide range of absorption bands, and the efficient generation of photocarriers in solar spectra at low intensities, make them suitable for light harvesting materials.[3–7] Particularly, metal–free azo–dyes such as methyl red (MR) have unique optoelectronic properties originating from delocalized photoexcited carriers from a lone pair of electrons existing in them, and, thus, they have recently attracted significant interests for solar cell devices.[3,12–15]

On the other hand, dye–molecules usually form various aggregates in thin films due to π–π interactions, which may affect the structural and spectral properties of the films as well as the performance of dye–based photovoltaic devices.[3,16–19] Previously, extensive efforts have been devoted to investigate the effects of aggregates on the optoelectronic properties of dye films using various spectroscopic and microscopic techniques.[20,21] However, these studies usually showed only accumulative effects of all aggregates on the film without elaborating the nanoscale effects of individual ones. In this regard, the mapping of localized aggregates in a film and understanding their photophysical properties in an operational solar cell device still remain a challenging issue, though those are essential for the further improvement of dye–based optoelectronic device performances.

Herein, we report the nanoscale mapping of wavelength–dependent photoresponses in H– and J–aggregates of azo dye–based solar cell films using a wavelength–selective photoconductive noise microscopy. In this strategy, we quantitatively mapped the localized variations of conductivities (σ) and electronic trap densities in an azo–dye film by a conducting probe scanning on the surface while illuminating the lights with various wavelengths. The results showed localized individual domains exhibiting the wavelength–selective excitations of carriers, allowing us to identify the domains as H– or J–aggregates. Furthermore, we obtained wavelength–dependent maps of short–circuit currents (I_{sc}), photocurrents, and charge–trap densities in the aggregates of the dye–film. Interestingly, *the short-circuit currents* I_{sc} of the dye–based solar cells and *photoconductivities* $\Delta\sigma_{PC}$ of the dye–film exhibited power law dependences with *trap densities under illuminated conditions* (N_{T_L}) and *trap density change by illumination* (ΔN_T), respectively in both aggregates like $I_{sc} \propto N_{T\_L}{}^{-3/4}$ and $\Delta\sigma_{PC} \propto |\Delta N_T|^{1/2}$. The results were attributed to the carrier recombination process enhanced by charge–traps in the film, revealing that charge–traps are one

[a] Department of Physics and Astronomy, and Institute of Applied Physics, Seoul National University, Seoul, 08826, Korea. E-mail:seunghun@snu.ac.kr
† Footnotes relating to the title and/or authors should appear here.
Electronic Supplementary Information (ESI) available: [Current and noise maps of dye solar cell films]. See DOI: 10.1039/x0xx00000x

View Article Online
DOI: 10.1039/D0TA07328H

of the major factors determining the performances of dye–based solar cell devices. Importantly, J–aggregates exhibited a lower trap density than H–aggregates, and, thus, they had higher short–circuit currents as well as larger open circuit voltages, indicating that J–aggregates are favorable structures for a solar cell application. Our method allowed us to map the nanoscale optoelectronic properties of solar cell films in a wavelength selective manner and provided an important guideline in improving the performance for solar cell devices based on the film. Thus, it can be a powerful tool for both basic researches and applications for optoelectronic devices based on dye molecules.

2 Results and discussion

2.1 Wavelength–selective photoconductive noise microscopy set–up on dye-based solar cells

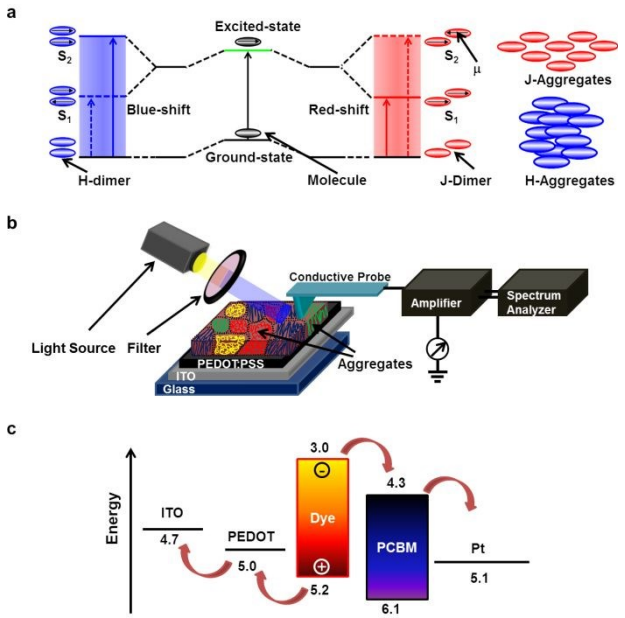

Fig. 1 Schematic diagram of a wavelength–selective scanning photoconductivity–noise measurement set–up and energy levels of a methyl red based solar cell film. (a) Photoexcitation diagram of J– and H– dimers (aggregates). (b) Experimental set–up for the wavelength selective scanning photoconductive–noise microscopy on a MR based solar cell. (c) Diagram showing the energy levels of the MR–PCBM bulk heterojunction solar cell.

Fig. 1a shows an optical excitation diagram of different dye aggregates. When two molecules come close, they form a dimer to minimize their energy, and the overlap of electronic wave functions results in the splitting of energy levels as shown in the diagram.[21] It was previously reported that two dye molecules could align in a *parallel* (face–to–face stacking) or a *head–to–tail* arrangement (end–to–end stacking).[21] A *parallel* or a *head–to–tail* stacking of two molecules is known as a *H*– or a *J*–dimer, which leads to the formation of *H*– or *J*–aggregates, respectively (Fig. 1a). The formation of H–aggregates may require a high density of molecules, because the effective overlaps between molecules are much larger in H–aggregates than those in J–aggregates. When the lights of a suitable wavelength are illuminated, electrons in the dye molecules can be excited to the higher energy levels of antibonding orbitals. The parallel transition dipoles (face–to–face) of H–aggregates produce a blue shift in the transition spectrum as formulated by the molecular exciton theory.[21] Conversely, the staggered (head–to–tail) transition dipoles of J–aggregates produce a red shift in the transition spectrum. MR dye films have shown a rather large cluster size by molecular assembly due to strong intermolecular π–π interactions and substrate–MR interactions, resulting in a well-packed formation of stable J– and H–aggregates with different photo-excitation and noise properties.[12,22–25] Due to such stable aggregates with versatile properties, MR dye films can be an ideal sample for the researches to develop a new analysis tool for mapping the wavelength-dependent photophysical properties of such microstructures in solar cell films and their effects on a solar cell efficiency.

Fig. 1b is the schematic illustration showing our experimental set–up for the mapping of wavelength–selective local photocurrents and charge–trap activities on the dye–based solar cell film. The details of a solar cell fabrication and photoconductive noise microscopy measurements are described in the Experimental Section. In brief, the MR–Phenyl–C61–butyric acid methyl ester (PCBM) film of ~80 nm thickness was prepared on the poly(3,4-ethylenedioxythiophene):polystyrene sulfonate (PEDOT:PSS)–coated indium tin oxide (ITO) glass via a solution process strategy.[26–28] The dye–PCBM layer acted as a photoactive material, while the PEDOT:PSS coated ITO layer worked as a hole–collecting layer.[29] For the photoconductive noise microscopy measurements, a Pt–based conducting probe installed on the conducting atomic force microscopy (AFM) (XE–70, Park Systems) made a direct contact with the dye–PCBM film and was used to measure the electrical currents through it. Further, we integrated a wavelength controllable light source with the AFM set–up enabling wavelength selective photoconductive noise measurements.[28,30–32] Here, the local currents and current noises through the probe were measured while the film was illuminated by lights with different wavelengths. The measured current noises were analyzed by the home–built spectrum analyzer, a band pass filter, and a RMS–to–DC converter.[33,34] By scanning the probe over the film, we were able to obtain the maps of the local currents and electrical noises of the same area, simultaneously. The measured maps were analyzed to obtain the distribution maps of the conductivity and the charge–trap density. The photoconductive noise microscopy can provide a comprehensive picture of photo–induced charge transports and charge–trap activities in solar cell films.

Fig. 1c is an energy–level diagram of the MR–PCBM bulk heterojunction solar cell. The energy diagram shows the conduction band minimum (CBM) and the valence band maximum (VBM) of MR and PCBM along with the Fermi levels of the Pt tip and the ITO electrode. By the light illumination, the electrons of the MR dye, the strong absorber of the visible spectrum, are excited from the valance band to the conduction

View Article Online DOI: 10.1039/D0TA08738H

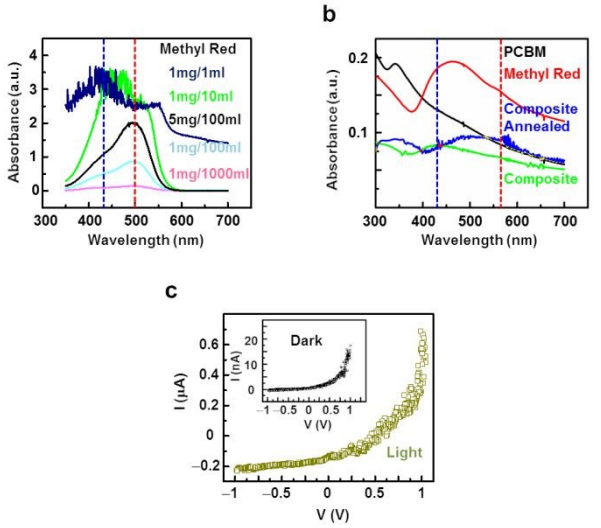

Fig. 2 Optical characteristics of methyl red dye and the solar cell film. (a) Concentration dependence optical absorption spectra of the methyl red (MR) dye in dichlorobenzene solvent, showing formation of aggregates. (b) Absorption spectra of films of pristine MR, PCBM and the mixture of MR:PCBM (1:1) prepared under similar conditions. (c) Current–Voltage (I–V) curves in dark and light–illuminated conditions, providing evidence of photovoltaic characteristics.

band through the transitions from bonding orbitals to anti–bonding orbitals such as n–π* and π–π*,[12,17] leaving holes in the valance band. The excited electrons at the CBM of MR (~–3 eV) can be easily transferred to the CBM of PCBM which is a lower energy level (~–4.3 eV). The electrons are finally collected at the metal electrode. The holes at the VBM of MR dye (~5 eV) are favorably collected by the PEDOT:PSS–coated ITO due to the lower Fermi level of the ITO (~4.7 eV) as compared to the VBM of MR.

2.2 Optical characterization of methyl red dye and dye based solar cell films

Fig. 2a shows UV–Visible absorption spectra of the MR dye in a dichlorobenzene (DCB) solution at various MR concentrations. Here, MR (10 mg) was first dissolved in DCB (10 ml) by applying a sonication for 90 minutes. And, the UV–Visible spectra were measured in a 350–700 nm range by an Agilent 8430 spectrophotometer. The UV–visible spectra of the dilute solutions (~1μg/l) exhibited an absorption maximum peak (λ_{max}) at ~490 nm which is close to the λ_{max} (~484 nm) of an individual strand of the MR dye.[35] As the concentration of the MR was increased, another absorption peak with a relatively low intensity appeared at the wavelength of ~430 nm. However, at high concentrations (~1 mg/ml), the peak at the 430 nm became prominent and blue–shifted. In previous reports, a very dilute solution or an individual strand of MR dye shows a peak near ~500 nm, while the absorbance peak near ~430 nm becomes prominent at a high concentration solution possibly due to the formation of H-aggregates, which is consistent with our results.[35–39] It should also be noted that the peak at a rather long wavelength of ~490 nm showed a tendency of a red–shift, whereas the one with a rather short wavelength of ~430 nm showed a blue shift as the concentration of the MR was increased in the solution from ~1 μg/l to ~1 mg/ml. Overall, the absorption spectra and peaks of the dye were strongly dependent on the concentration of the dye in the solution. The blue and red shifts in the respective peaks could be attributed to the formation of aggregates in the concentrated solution.[1,17,19–21,35] When small molecules come close to each other, they interact through transition dipoles and form aggregates, resulting in an overlap of the molecular orbitals and electronic wave functions.[20,21] These lead to two characteristic peaks in the absorption spectra of the dye molecules. One peak gets blue–shifted (hypsochromic), whereas another peak is red–shifted (bathochromic) when compared with the absorption peak of a monomer molecule. The molecular aggregates depending on their *side–wise* or *head–to–tail* alignments are commonly denoted as *H*–aggregates (or hypsochromic–aggregates) or *J*–aggregates (or bathochromic–aggregates), causing *hypsochromic* or *bathochromic* absorption peaks, respectively. It is worth mentioning that previous works report the emission spectra of MR dye exhibiting the *mirror-image* characteristics of those of the absorption spectra.[37,40,41] The emission spectra were reported to have two peaks at 450 nm and 600 nm, and the dominant peak showed a red shift at an increased dye concentration, which is somewhat consistent with our optical measurement data.[37,40,41] Our results show that dye films include H– and J–aggregates, and inter–molecular interactions play a decisive role in the photophysical properties of the film as reported previously.[21]

Fig. 2b shows UV–Visible absorption spectra of the thin films of *MR, PCBM* and *MR–PCBM* blend spun on glass substrates, which are plotted with *red, black* and *green* colours, respectively. The details of the film preparation method are described in the Experimental Section. The UV–Visible spectra were measured in the range of 300–700 nm by an Agilent 8453 spectrophotometer. The MR (graph plotted with red line) showed two absorption peaks at ~450 and ~550 nm, which were similar to the absorption peaks of the concentrated solution of MR as shown in the Fig. 2a. This implicates that J– and H–aggregates were also formed in the solid state. Notably, the intensity of the absorption peak of the H–aggregate was higher than that of the J–aggregate, indicating the large fraction of H–aggregates. The PCBM film (graph plotted with black coloured lines) showed an absorption peak in the UV–region (~350 nm) as reported previously.[32] We could not observe the formation of any aggregates in the PCBM film spun from the 1 mg/ml solution in DCB, presumably due to the non–linear structure of the PCBM and a lack of π–π interactions as reported previously.[42] The spun film from the mixture of dye–PCBM exhibited an intense peak at ~450 nm predominantly due to the formation of H–aggregates.[35,41] The intensity of the peak due to J–aggregates was negligibly small, implicating a low fraction of J–aggregates in the film. However, after annealing the sample at 130 °C for 90 minutes, we observed the recovery of a bathochromic peak (graph plotted with blue line) with the broad range of absorption in a visible regime. It implies that the annealing process enabled the rearrangement of molecules in

View Article Online
DOI: 10.1039/D0TA07328H

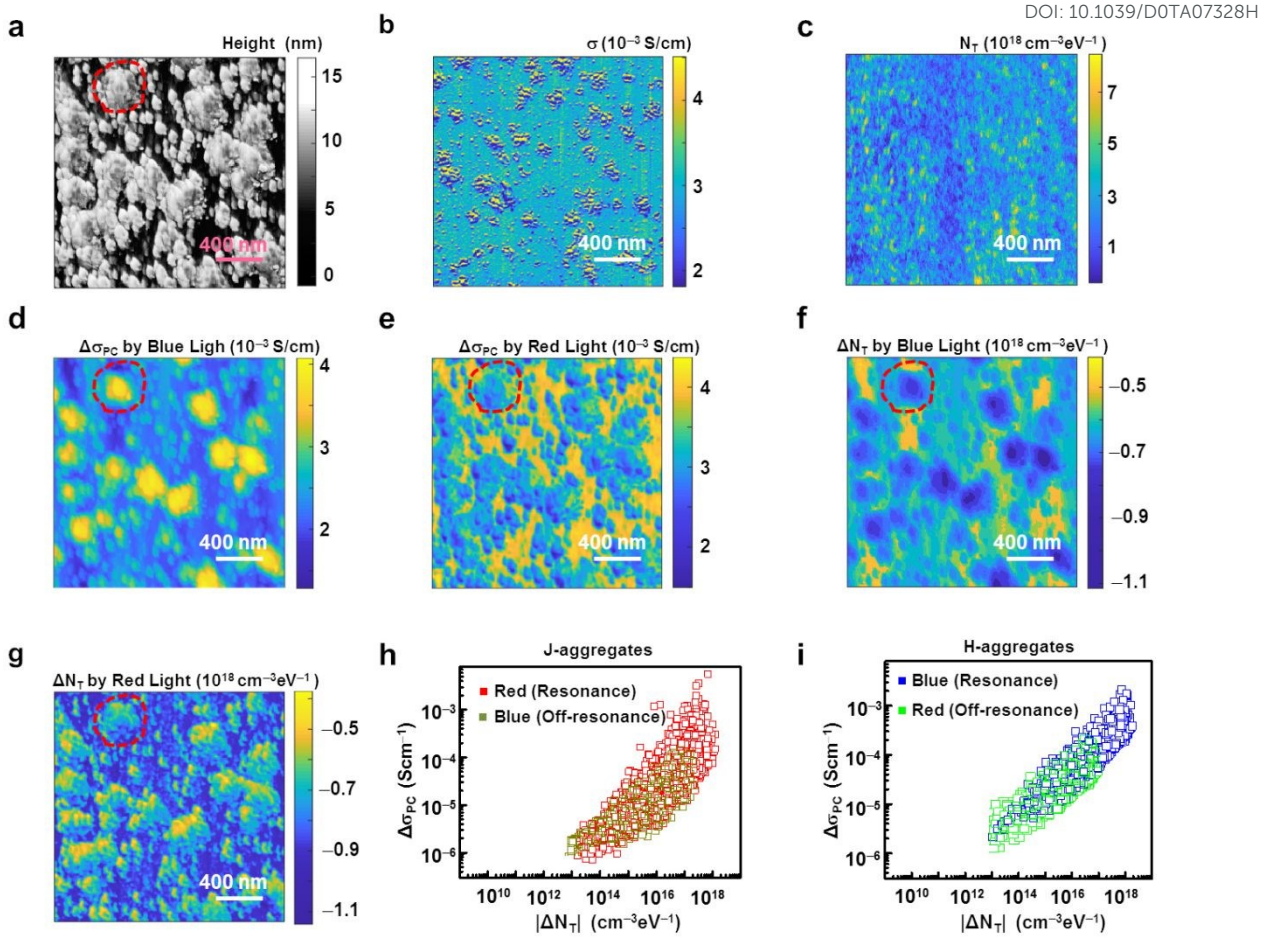

Fig. 3 Wavelength dependent photoconductive mapping in H– and J– aggregates of a solar cell film. (a) AFM topography image of the surface of the solar cell film showing two kinds of structures. (b) Dark current map measured at 0.1 V. (c) Normalized noise power spectral density map of same region as the current map. (d) Photoconductivity map measured at 0.1 V while the film was illuminated with blue lights of wavelength ~450 nm. (e) Photoconductivity map measured at 0.1 V while the film was illuminated with red lights of wavelength ~600 nm. (f) Change in trap density map by blue light. (g) Change in trap density map by red light. (h) Scatter plots showing photoconductivity dependence on the trap density change by illumination in resonance and off–resonance cases in J–aggregates. (i) Scatter plots showing photoconductivity dependence on trap density change by illumination in resonance and off–resonance cases in H–aggregates.

the thin film presumably due to the evaporation of the trapped solvent, leading to the reemergence of J–aggregates. These results indicate that the microstructures of our dye films can be tuned externally by providing a physical or chemical treatment to the film.[1,12]

Fig. 2c shows the current–voltage (I–V) characteristics of a solar cell film measured with (olive colored line) or without (inset graph) the illumination of the white light (intensity ~100 mW-cm^{-2}). Here, the currents were measured through the MR–PCBM film between the Pt electrode and an electrically–grounded PEDOT:PSS–coated ITO substrate. In the dark conditions, a typical asymmetric I–V curve of a junction behaviour was observed with a very low reverse bias current.[28] When the film was illuminated with white lights, the currents increased significantly as compared to currents in the dark condition, implying the generation of photoexcited carriers. In addition, even at the zero external bias, we observed a nearly 100 nA of short-circuit currents, showing the proper operation as a solar cell. The open circuit voltage (V_{OC}) measured at the zero current value was close to 500 mV. Presumably, the large band gap of the MR makes the dye suitable for solar cell applications with a large open circuit voltage.[43]

2.3 Mapping effects of charge–traps on photoconductivity in aggregates of dye–based solar cell films in resonance and off-resonance cases

Fig. 3a shows an AFM topography image of an MR–PCBM film on the PEDOT:PSS–coated ITO substrate in a solar cell configuration. The 1 μN of contact force was maintained to provide a good contact between the probe and the film surface during imaging. The topography image shows a height variation in the film due to the formation of the domains of ~500 nm sizes, which were similar to previous results.[18] We could repeatedly image the surface without any changes in the topography, indicating the stable formation of our films.[15–17]

A local conductivity map measured in a dark condition on the same region as in the Fig. 3a, is shown in the Fig. 3b. Here,

View Article Online DOI: 10.1039/D0TA07328H

we first measured a current map at the bias voltage of 0.1 V (Fig. S1, Electronic Supplementary Information (ESI)) and used it to calculate the conductivity (σ) map using the method reported previously.[26,27] The details of the calculation method are described in the Experimental and method sections. In brief, we assumed that charge carriers flowed mainly in a vertical direction from the ITO electrode to the conducting probe through the dye film, and parasitic currents in a lateral direction inside the film was limited due to the low conductivity of the dye film. In this case, a conductivity can be written as $\sigma = Id/(VA)$, where *I, d, V*, and *A* represent *a measured current, the thickness of the film, an applied voltage*, and *the contact area of a conducting probe*, respectively. The estimated local conductivity map indicates a stable electrical contact between the tip and the film regardless of the topological roughness of the dye film (MR–PCBM). The film showed the conductivity up to 10^{-3} Scm^{-1} which was similar to the previously observed values in PCBM films.[44] Notably, we did not observe any correlation between the topography and the conductivity maps, indicating that the conductivity variation came from the electronic properties of aggregates rather than the surface roughness.

Fig. 3c shows a distribution map of charge–trap density under dark conditions (N_T) obtained from the noise and current maps (Fig. S1 and S2, ESI) which were measured simultaneously on the same region as in Fig. 3a. The details of N_T calculations are described in the Experimental Section.[26,27] Note that the N_T showed a rather large value with some random variations as large as 10^{18} $cm^{-3}eV^{-1}$.[26,27] Presumably, in an organic materials such as a dye, electrical noises can be generated by various localized traps such as defects, impurities, entanglements, disorders, and structural inhomogeneities, resulting in high N_T.[26–28,45,46]

Fig. *3d* and *3e* show photoconductivity maps in the same region as in the Fig. 3a while illuminated by the lights with the wavelengths of *450* and *600 nm*, respectively. Here, we measured the current map at 0.1 V with a specific wavelength light filtered from the white light of the power of 100 $mW–cm^{-2}$. The measured current map was subtracted by the corresponding current map in the dark condition to obtain the photocurrent map, from which we estimated photoconductivity map as explained in the description of Fig. 3b. Note that the domains with relatively *high heights* (protruded regions marked by red dotted circle in the topography image Fig. 3a) exhibited high photoconductivities when illuminated with the blue lights of the wavelength *450* nm. To the contrary, the complementary domains with relatively *low heights* showed high photoconductivities with the red lights of the wavelength *600* nm. On the basis of correlation between the topography and photoconductivity maps, we could envisage the formation of different kind of aggregates with different resonance absorption wavelengths at the sub–micron level. More specifically, the domains showing high photoconductivities at excitation wavelength of *450 nm* or *600 nm* could be attributed to the regions with *H*– or *J*–aggregates, respectively, as their carriers can be easily excited by the resonance wavelengths.[1,17] These results are in accordance with the absorption spectra (Fig. 2a,b) where we observed two different absorption peaks corresponding to H– and J–aggregates.[35–37]

Fig. *3f* and *3g* shows the mapping of the charge–trap density change ΔN_T measured on the same region as in the Fig. 3a when illuminated with lights of wavelengths *450 (blue)* and *600 (red)* nm, respectively. In the case of the *blue* light illumination to the dye film (Fig. 3f), *protruded regions (H–aggregates)* showed a relatively large decrease in the trap density. Similarly, the trap density decrement was large in *lower height regions (J–aggregates)* when the film was illuminated with the *red light* (Fig. 3g). Significantly, there was an overall decrease in the trap density by ~5×10^{17} cm^{-3} eV^{-1} when the dye film was illuminated with blue or red lights. These results show that the resonance absorption of lights induced larger decrease in the trap density than non–resonance absorption in both H– and J–aggregates. Presumably, the excess resonant photocarriers could have filled the charge–traps, resulting in an overall decrease in the trap density.[47]

Fig. *3h* and *3i* are scattered plots showing the photoconductivity dependence on the trap density change by the illumination of lights with the wavelengths of *450* and *600 nm*, in *J*– and *H*–aggregates, respectively. The *red (green)* and *dark yellow (blue)* coloured plots in Fig. 3h (3i) showed the dependence for *red* and *blue* lights, respectively, in J– (–H) aggregates. Each data point shows a pair of photoconductivity and trap density change by the illumination at the same location in the maps of the dye film. Note that, regardless of resonance and off–resonance cases in J– and H–aggregates, the photoconductivity was found to be directly proportional to the 0.5 power of the modulus of the trap density change by the illumination of lights like $\Delta\sigma_{PC} \propto |\Delta N_T|^{1/2}$. Plausibly, the dependence can be explained by trap–assisted recombination process model as reported previously.[28,48] Briefly, the change in conductivity $\Delta\sigma_{PC}$ can be mathematically expressed as,

$$\Delta\sigma_{PC} = e\mu_L n_L - e\mu n = e(\mu+\Delta\mu)(n+\Delta n) - e\mu n = e\mu\Delta n + en\Delta\mu + e\Delta\mu\Delta n, \quad (1)$$

where n and μ are carrier density and mobility, respectively. The subscript *L* denotes *illuminated* conditions. A trap density N_T under dark conditions can be expressed in terms of the mobility μ as, $N_T \cong A.\mu^{-2}$ as formulated by an effective medium approximation theory, where *A* is a proportionality constant depending only on effective hopping energy.[26,49] Thus, a trap density N_{T_L} under illuminated conditions can be written as $N_{T\_L} \cong A.(\mu+\Delta\mu)^{-2}$. An illumination can affect a trap density by a large extent, and it can also bring some small change in a mobility.[50,51] Assuming, $\Delta\mu/\mu << 1$ and applying Taylor expansion to N_{T_L}, we can obtain

$$\Delta N_T \equiv N_{T-L}(\mu) - N_T(\mu) \cong A.\frac{1}{\mu^2}.\left(1+\frac{\Delta\mu}{\mu}\right)^{-2} - A.\mu^{-2} \cong -2A.\frac{\Delta\mu}{\mu^3} .\cong -2A.\frac{\Delta\mu}{A^{3/2}N_T^{-3/2}} \quad (2)$$

Thus, $\Delta\mu$ dependence on N_T can be approximated as

$\Delta\mu = -A^{\frac{1}{2}}.\frac{1}{2}.N_T^{-\frac{3}{2}}.\Delta N_T$. Substituting μ and $\Delta\mu$ values in Eqn. (1), we can obtain

View Article Online
DOI: 10.1039/D0TA07328H

$$\Delta\sigma_{PC} = eA^{1/2}N_T^{-1/2}\Delta n - \frac{1}{2}eA^{1/2}nN_T^{-\frac{3}{2}}\Delta N_T - \frac{1}{2}eA^{1/2}N_T^{-3/2}\Delta N_T\Delta n. \quad (3)$$

Let us assume that n'and p' are *electron* and *hole* densities in the material, respectively. Also N_T is the total trap density out of which N_{Tp} and N_{Te} are traps occupied by *holes* and *electrons*, respectively. Then, the charge neutrality requires[52,53]

$(n' - p') + (N_{Te} - N_{Tp})=0.$ (4)

On illumination, we have the change in the respective quantities by Δn', Δp', ΔN_{Te} and ΔN_{Tp}.

$\{(n'+\Delta n') - (p'-\Delta p')\} + \{(N_{Te}+\Delta N_{Te}) - (N_{Tp}-\Delta N_{Tp})\}=0$ (5)

$\Delta n'+\Delta p' + \Delta N_{Te}+\Delta N_{Tp}=0$, or $\Delta n +\Delta N_T =0$, $\Delta n = -\Delta N_T$, (6)

where $\Delta n = \Delta n'+\Delta p'$ is the total change in the carrier density, and $\Delta N_{Te}+\Delta N_{Tp} = \Delta N_T$ is the total change in the trap density. By substituting $\Delta n = -\Delta N_T$, Eqn. (3) can be modified as

$$\Delta\sigma_{PC} = -eA^{1/2}N_T^{-\frac{1}{2}}\Delta N_T - \frac{1}{2}eA^{1/2}nN_T^{-\frac{3}{2}}\Delta N_T + \frac{1}{2}eA^{1/2}N_T^{-3/2}\Delta N_T\Delta N_T. \quad (7)$$

Experimentally, we observed the dramatic reduction of trap density under illumination. Plausible explanation can be the filling of traps by photocarriers. Analytically, change in trap density make a shift in the Fermi level by the photocarriers.[52,53] Thus, at a higher trap density location, screening in trap density would be rather large due to the filling of the traps by the photocarriers, resulting in the larger trap density change at larger N_T values.[52,53] Therefore, $|N_T| \propto |\Delta N_T|$. Also, we observe a similar behavior (Supplementary Fig. S3). Thus, $|N_T|$ in Eqn. (7) can be substituted by $C|\Delta N_T|$. Then, Eqn. (7) can be modified as

$$\Delta\sigma_{PC} = -eCA^{\frac{1}{2}}|\Delta N_T|^{1/2} - \frac{1}{2}eCA^{\frac{1}{2}}n|\Delta N_T|^{-1/2} + \frac{1}{2}eC^2A^{\frac{1}{2}}|\Delta N_T|^{1/2}. \quad (8)$$

On an average, ΔN_T (10^{14} ~10^{18} $cm^{-3}eV^{-1}$) is much larger than the initial carrier density n under dark conditions (<<10^{12} $cm^{-3}eV^{-1}$) in a dye,[54] which holds in our cases. Therefore, we can neglect 2nd term in the Eqn. (8), and Eqn. (8) can be further simplified as

$$\Delta\sigma_{PC} = -eCA^{\frac{1}{2}}(1-\frac{C}{2})|\Delta N_T|^{\frac{1}{2}} \quad (9)$$

So,

$$\Delta\sigma_{PC} = D|\Delta N_T|^{1/2} \quad (10)$$

where $D=(eC)A^{1/2}(C/2-1)$ is a constant. Eqn. (10) explains the dependence of photoconductivity on the trap density change by illumination, which is consistent with our observations in the resonance and off–resonance cases of various aggregates. The strong dependence between photoconductivity and change in trap density indicates that the suppression of traps is an important parameter to enhance the photoconductivity, and in turn, it may enhance the performance of a solar cell device.

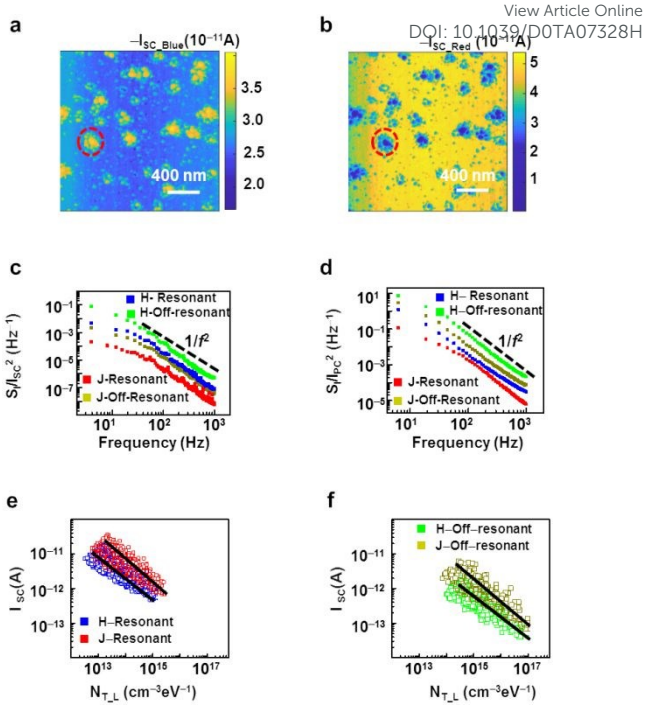

Fig. 4 Mapping of short–circuit currents and noises in aggregates of dye solar cell films. (a) Map of short–circuit currents when the film was illuminated with blue light measured without an external bias (b) Map of short–circuit currents when film was illuminated with red light measured without an external bias. (c) Scattered plots showing the dependence of short–circuit noise power spectral density on frequency in J– (H–) aggregates in resonance or off–resonance cases at a zero bias, plotted with red or dark–yellow (blue or green) colour symbols, respectively. (d) Scattered plots showing the dependence of noise power spectral density on frequency in J– (H–) aggregates in *resonance* or *off–resonance* case at a bias voltage of 0.1 V, plotted with *red* or *dark–yellow* (blue or green) colour symbols, respectively. (e) Scattered plots showing the dependence of short–circuit current under illuminated conditions in resonance cases of *J–* and *H– aggregates* plotted with *red* and *blue* colour symbols, respectively. The short–circuit currents were inversely proportional to the ~0.75 power of the illuminated trap densities in *J–* and *H–* aggregates, separately. (f) Scattered plots showing the dependence of short–circuit current on trap density under illuminated conditions in off–resonance cases of *J–* and *H-aggregates* plotted with *dark-yellow* and *green* color symbols, respectively. The short-circuit currents were inversely proportional to the ~0.75 power of the illuminated trap densities in J– and H– aggregates, separately.

2.4 Mapping of resonant and off–resonant short–circuit currents in H– and J–aggregates

In our experimental set–up, the dye films with an underlying ITO electrode and a conducting AFM probe formed a *solar cell structure*. Thus, we can map the short–circuit currents on the different regions of the dye film to estimate the efficiency of the regions as a solar cell component. Fig. *4a* and *4b* are short–circuit current maps on the dye solar cell film while illuminated with *blue (450 nm)* and *red (600 nm)* lights, respectively. In this work, we mapped the wavelength dependent photocurrents with a zero bias voltage while illuminating with specific wavelength lights. The average level of the short–circuit current was ~*2.5* and *3.5* pA (current density ~1 mA–cm^{-2}) under *blue* and *red* lights, respectively. These currents are typical values for a MR dye–based heterojunction

View Article Online
DOI: 10.1039/D0TA07708H

solar cell.[15] Note that the domains showing a *larger* short–circuit currents with *blue* lights (marked with red dotted circle) exhibited *smaller* currents with *red* lights and *vice–versa*. These results indicate that the domains with high short–circuit currents on illumination with *blue* or *red* lights can be attributed to the formation of *H*– or *J*–aggregates, respectively. In the resonance cases, both types of domains showed currents of order of ~10 pA, whereas the off–resonant currents were less than ~1 pA. Presumably, in a resonance absorption case, a high absorption cross section and an efficient inter–molecular transfer of energy between the molecules make efficient conversion of photons into photocurrents.[26,55] Notably, with both on– and off– resonance cases, the short–circuit currents in J–aggregates was higher than those in H–aggregates. Previous works show that J–aggregates have better efficiencies in converting photons to currents in comparison to H–aggregates.[20] The strong vibronic interactions in H–aggregates due to larger overlaps of molecules can lead to a faster decay of the excited carriers, making J–aggregates better for a short–circuit current generation. Importantly, our method allowed us to map the different efficiency of the aggregates in the dye film, providing important insights about the photoconductive properties in aggregates.

Fig. 4c shows the scattered plots for normalized noise power spectral density (PSD) S_I/I^2 spectra of short–circuit currents as a function of frequencies at a zero bias voltage. The S_I/I^2 was measured in J– aggregates (H–aggregates) of the dye film in *resonance* or *off–resonance* cases plotted with *red* or *dark–yellow* (blue or green) symbols, respectively. Here, the probe made a stationary contact with a specific position on the dye solar cell film, and the electrical currents were measured and analyzed using a fast Fourier transform (FFT) signal analyzer (SR770, Stanford Research Systems). All the measurements were performed in presence of blue or red lights. The slopes of all the curves of H– and J–aggregates (Fig. 4c) were close to ~–2 indicating that noise PSD followed *1/f*^{2} behavior. Previous works show that the noise PSD of traps of single relaxation time can be expressed by a Lorentzian function like $S_I/I^2 \propto 1/[1+(2\pi f\tau)^2]$, and the dependence approximates to $1/f^2$ at sufficiently high frequencies.[14]

Plausibly, in our film, the intermolecular electron–phonon (e–p) coupling in the aggregate of dye molecules could create the dominant trap states with an identical potential depth and relaxation time, resulting in *1/f*^{2} dependence.[56,57] It also should be noted that H–aggregates showed higher noise PSD values than J–aggregates. Presumably, the e–p coupling strength varies from one type of aggregates to another due to different intermolecular distance, resulting in different noise levels in various aggregates as reported previously.[56,57] In the H–aggregates, high packing densities of molecules could produce a strong e–p coupling due to formation of a large number of junction potentials (traps), causing a high noise level.[57,58] Interestingly, the S_I/I^2 was higher in off–resonance cases in comparison to resonance cases of J– and H–aggregates (Fig. 4c), which could be due to the strong e–p coupling in off–resonance cases. In off–resonance cases, there can be a spatial variation in the absorption cross section of the dye and a large absorption linewidth of the light, which can lead to the photocarrier inhomogeneity and enhanced e–p coupling resulting in a large number of trapping potentials.[55,58]

Fig. 4d shows the S_I/I^2 plot, the measure of the photocurrent fluctuations with an applied bias of 0.1 V as a function of frequencies. The experimental procedure was similar as described in Fig. 4c. The S_I/I^2 was measured in J– (H–) aggregates in the *resonance* or *off-resonance* cases of the dye film at an applied bias of 0.1V, plotted with *red* or *dark–yellow* (*blue* or *green*) symbols, respectively. Here, we also observed *1/f*^{2} noise behaviors in different aggregates for both resonance and off–resonance conditions. Notably, the resonance cases showed two orders of magnitude lower noise in comparison to off–resonance cases. Moreover, photocurrent noises were much higher (two orders) than the corresponding short–circuit noises. Presumably, an external bias could excite and inject additional carriers in the aggregates, creating high lattice distortion and significantly increased e–p coupling. That would result in the enhanced electrical noises.[59]

Fig. *4e* and *4f* are scatter plots showing the dependence of the short–circuit current on trap densities in *resonance* and *off–resonance* cases, respectively. The *red* and *blue* color symbols in the Fig. 4e represent resonance cases for *J*– and *H*–aggregates, respectively. Similarly, the *dark–yellow* and *green* color symbols in the Fig. 4f represent off–resonance cases for *J*– and *H*–aggregates, respectively. Each data point represents short–circuit current and corresponding trap density values of a single type of aggregates at a specific position. The results show that short–circuit currents I_{sc} were *inversely proportional* to the *~3/4* power of the trap densities under illuminated conditions N_{T_L} in both type of aggregates like $I_{sc} \sim N_{T\_L}^{-0.75}$. This behavior can also be explained by the trap–assisted recombination process. In the short–circuit condition with lights, the photocarriers generated in a solar cell should diffuse to the electrodes to contribute to a current. Here, the I_{sc} in the solar cell should be proportional to the multiplication of the generation rate of photocarriers (*G*) and the photocarrier collection length (L_c) of the solar cell like[60]

$$I_{sc} \propto (G \times L_c) \tag{11}$$

In our case, the *G* is proportional to the carrier density under illumination n_L which is inversely proportional to the $N_{T\_L}^{0.5}$ as shown in the previous report.[28] On the other hand, the L_c is approximately linearly proportional to carrier diffusion length (L_D) of the photoactive layer in the solar cell.[28,61] L_D is known to be proportional to the square root of the carrier lifetime (τ) as,[62]

$$L_D = \sqrt{D\tau} \tag{12}$$

where *D* is a carrier diffusivity. The carrier density n_L is inversely proportion to recombination rate.[28] The recombination rate is inversely proportional to carrier lifetime τ.[28] Hence, the n_L and τ have a direct correlation, and they are inversely proportional to the $N_{T\_L}^{0.5}$. So, L_D is inversely proportional to the $N_{T\_L}^{0.25}$. Then, from Eqn. (11), the short–circuit current I_{sc} should be inversely proportional to the $N_{T\_L}^{0.75}$ which agrees well with the measured result of $I_{sc} \sim N_{T\_L}^{-0.75}$ in both H– and J–aggregates.

3 Experimental and methods section

3.1 Materials and device fabrication

The methyl red dye (2– (4–Dimethylaminophenylazo) benzoic acid, 4–Dimethylaminoazobenzene–2–carboxylic acid) (Product ID 250198, Mw ~270), PCBM (Product ID 684449), and PEDOT:PSS (Product ID 655201) were purchased from Sigma–Aldrich. The low sheet resistance (~8 Ω/□) ITO glass was also obtained from Sigma–Aldrich (Product ID 703192). The 10 mg of each of the methyl red and PCBM were separately dissolved in 10 ml of 1,2 dichlorobenzene. They were dissolved by applying a sonication at 60 °C for 90 minutes. The prepared solutions were then mixed together and sonicated for another one hour to obtain the blend in a solution form. The blend solution was spin coated on the PEDOT:PSS–coated ITO substrate at 4000 rpm for 60 seconds. The dye film was heated at 130° C for 90 minutes.

3.2 Wavelength selective mapping of photocurrents and electrical noises

A Pt-based conducting probe (25Pt300B, Park Systems) installed on an AFM (XE-70, Park Systems) was approached and contacted to the surface of the dye solar cell film as described in the Fig. 1b. Here, the contact force of the AFM probe to the film surface was maintained as 1 μN via the contact force feedback loop of the AFM system. A *DC* bias voltage was applied between the AFM probe and the PEDOT:PSS on the ITO substrate using a function generator (DS345, Stanford Research Systems), and current signals through the probe were measured and amplified by a low–noise preamplifier (SR570, Stanford Research Systems) connected to the probe. The amplified current signals were filtered by a band–pass filter included in the preamplifier to obtain the electrical noise signal which is the fluctuating component of the current signals. The RMS power of the noise signal could be obtained using a RMS–to–DC converter built using an AD737 chip (purchased from Analog Devices). Note that the obtained noise power is the integrated value of the noise PSDs over the frequency range of the pass band of the used band–pass filter. Finally, we get the noise PSD value at the central frequency of the pass band by dividing the measured noise power with the bandwidth of the band–pass filter. By scanning the AFM probe on the dye film surface, we could obtain the current and noise PSD maps, simultaneously. Further, we measured a current map while illuminating a filtered (wavelength selected) light using a light source (LS-F100HS) and compared the map with that obtained at a dark condition to estimate a photocurrent map. The optical filters (supplied by Edmund Optics, Product Id 88-700) of bandwidth 25 nm and optical density ~4 (transmitted intensity attenuated by 10^4) were used for a wavelength selection.

3.3 Calculation of conductivities of dye solar cell films

Since the conductivity of the dye solar cell film was rather low, we can assume that charge carriers mainly flowed in a vertical direction from an underlying ITO substrate to a conducting probe through the film layer, and parasitic currents in a lateral direction inside the layer were limited. Thus, we calculated the conductivity of the dye film assuming a vertical charge transport. In this case, a conductivity σ can be calculated using $\sigma = Id/(VA)$, where I, d, V and A represent a *measured current*, the *thickness of the film*, an *applied voltage*, and the *contact area of a conducting probe*, respectively. In our experiment, the thickness of the film was ~80 nm. The contact area A of our conducting probe was estimated as ~2000 nm^2 from the effective contact radius.[34]

3.4 Calculation of charge–trap density in dye solar cell films

In this measurement, electrical currents flowed vertically between a conducting AFM tip and an underlying ITO film. Thus, the majority of electrical noises should be generated by the charge–traps inside the small volume of the dye film between the ITO electrode and the conducting AFM tip. Then, the PSD of the mean–square fluctuation in the number of occupied charge–traps in the small segment of the dye film within the contact area A of the tip can be written as[63,64]

$$S_{N_T}(f,x,y) = A \cdot \int_{-\infty}^{\infty}\int \frac{4\tau(E,x,y,z)}{1+[2\pi f\cdot\tau(E,x,y,z)]^2}\cdot f_t(1-f_t)\cdot N_T(E,x,y,z)\cdot dz\cdot dE \quad (13)$$

where the N_T, τ, and f are the *density of charge–traps over the space and energy*, a *trapping time constant*, and a *frequency*, respectively. The integral over z ranged from 0 to the dye-film thickness d. The trap occupancy function can be written as $f_t(E) = [1+\exp\{(E-E_f)/kT\}]^{-1}$ where E_f is Fermi level. At a rather low temperature condition including a room temperature, $f_t(1-f_t)$ behaves like a delta function around the Fermi level E_f, and the Eqn (13) after the integral over E can be simplified as[63,64]

$$S_{N_T}(f,x,y) = A\cdot kT\cdot\int \frac{4\tau(E_f,x,y,z)}{1+[2\pi f\cdot\tau(E_f,x,y,z)]^2}\cdot N_T(E_f,x,y,z)\cdot dz \quad (14)$$

Assuming that charge–traps are distributed uniformly over the z direction, the Eqn. (14) can be approximated as

$$S_{N_T}(f,x,y) = A\cdot d\cdot kT\cdot N_T(x,y)\frac{4\tau(x,y)}{1+[2\pi f\cdot\tau(x,y)]^2} \quad (15)$$

The noise PSD ΔS_I can be written as

$$S_I(f,x,y) = \frac{(I)^2}{(\Delta C)^2}S_{N_T}(f,x,y)\,, \quad (16)$$

where ΔC is the carrier number in the segment of the dye film. Then, the charge–trap density N_T can be written like,

$$N_T(x,y) = S_I(f,x,y)\frac{(\Delta C)^2}{(I)^2}\cdot\frac{1}{A\cdot d\cdot kT}\cdot\frac{1+[2\pi f\cdot\tau(x,y)]^2}{4\tau(x,y)} \quad (17)$$

The *average trapping time* τ and the *carrier density* in the dye were reported as ~10^{-5} seconds and ~10^{12} cm^{-3}eV^{-1}, respectively.[54,65]

3.5 Measurement of UV-Visible absorption spectra

View Article Online
DOI: 10.1039/D0TA07328H

UV-Visible absorption spectra of our films were measured using an Agilent 8453 spectrophotometer, where *deuterium-discharge* and *tungsten filament lamps* were used to get *UV* and *visible* ranges of lights, respectively. For the measurement, MR solution with a known concentration was poured inside a quartz cuvette, and the absorbance spectra were recorded in the transmittance mode. Here, the incident or reference light intensity (P_0) through a solvent filled cuvette was first measured. Then, the intensity P of lights through the dye solution was measured. The transmittance (T) was measured as the ratio of the output intensity like P/P_0. From the Beer-Lambert Law, the absorbance intensity *A* is estimated as –logT or $\log(P_0/P)$.[66] For a dye solution with a high concentration, the transmittance became very small, and the noise level of the photodetector began to affect the measured absorption signals. Thus, we observed a rather large noise level in the absorbance spectra, determining the detection limit of our absorption measurements.

4 Conclusions

We successfully performed the nanoscale mapping of the H– and J–aggregates and their photovoltaic activities in a dye solar cell film using a wavelength–selective photoconductive noise microscopy. The H– and J–aggregates could be identified in photoconductive mapping by their characteristic excitations by selective–wavelength illuminations. Interestingly, the *H– or J–*aggregates showed enhanced formations of photocarriers at *450* nm or *600* nm of wavelength, respectively, resulting in high photoconductivities and low charge–traps. Furthermore, we observed that the photoconductivity significantly depended on the charge–trap density change by the illumination of aggregates in the film, and they showed a power–law relationship like $\Delta\sigma_{PC} \propto |\Delta N_T|^{1/2}$ for each individual wavelengths illumination. Further, we observed that the wavelength dependent short–circuit currents of the dye solar cell was inversely proportional to the 3/4 power of the trap density under illuminated conditions, which reveals that the photocarriers and their recombination by charge–traps can be the major factor governing the performance of dye solar cell films. Importantly, J–aggregates showed higher short–circuit currents and larger open circuit voltages due to lower levels of the trap density, making J–aggregates favorable structures for solar cell applications. Since our method allows one to map the nanoscale wavelength–dependent photovoltaic activities in various microstructures of a solar cell film, it can be a powerful tool for both basic researches and applications of photoelectronic devices.

Conflicts of interest

There are no conflicts to declare.

Acknowledgements

This work was supported by BioNano Health-Guard Research Center funded by the Ministry of Science, ICT (MSIT) of Korea as Global Frontier Project (No. 2013M3A6B2078961). S.H. also acknowledges the support from National Research Foundation Korea grants (Nos. 2017R1A2B2006808, 2020R1A2B5B02002152) and the European Research Council under the European Union's Horizon 2020 research and innovation programme (grant agreement no. 0682286).

Notes and references

1 A. Liess, A. Arjona-Esteban, A. Kudzus, J. Albert, A.-M. Krause, A. Lv, M. Stolte, K. Meerholz and F. Wurthner, *Adv. Funct. Mater.*, 2018, **28**, 201805058.
2 L. Gao, C. Ge, W. Li, C. Jia, K. Zeng, W. Pan, H. Wu, Y. Zhao, Y. He, J. He, Z. Zhao, G. Niu, X. Guo, F. P. G. De Arquer, E. H. Sargent and J. Tang, *Adv. Funct. Mater.*, 2017, **27**, 1702360.
3 L. Zhang and J. M. Cole, *J. Mater. Chem. A*, 2017, **5**, 19541.
4 M. Freitag, J. Teucher, Y. Saigili, X. Zhang, F. Giordano, P. Liska, J. Hua, S. M. Zakeeruddin, J.-E. Moser, M. Gratzel and A. Hagfeldt, *Nat. Photonics*, 2017, **11**, 372.
5 B. E. Hardin, E. T. Hoke, P. B. Armstrong, J.-H. Yum, P. Comte, T. Torres, J. M. J. Frechet, M. K. Nazeeruddin, M. Gratzel and M. D. McGehee, *Nat. Photonics*, 2009, **3**, 406.
6 O. Brain and M. Gratzel, *Nature*, 1991, **353**, 6346.
7 H.-C. Su, Y.-Y. Wu, J.-L. Hou, G.-L. Zhang, Q.-Y. Zhu and J. Dai, *Chem. Commun.*, 2016, **54**, 4072.
8 L. Zhou, R. Wang, C. Yao, X. Li, C. Wang, X. Zhang, C. Xu, A. Zeng, D. Zhao and F. Zhang, *Nat. Commun.*, 2015, **6**, 6938.
9 X. Munoz-Berbel, R. Rodriguez-Rodriguez, N. Vigues, S. Demming, S. Buttgenbach, E. Verpoorte, P. Ortiz and A. Lloobera, *Lab Chip*, 2013, **13**, 4239.
10 J. Kim, H. Yoo, V. A. PhamBa, N. Shin and S. Hong, *Sci. Rep.*, 2018, **8**, 11958.
11 K. Yamjala, M. S. Nainar and N. R. Ramisetti, *Food Chem.*, 2016, **192**, 813.
12 M. M. Makhlouf and A. El-Denglawey, *Jpn. J. Appl. Phys.*, 2018, **57**, 042401.
13 E. N. Cho, D. Zhitomirsky, G. G. D. Han, Y. Liu and J. C. Grossman, *Appl. Mater. Interfaces.*, 2017, **9**, 8679.
14 D. Cho, M. Yang, N. Shin and S. Hong, *Nanotechnol.*, 2018, **29**, 11958.
15 S. Saha and N. B. Manik, *Thin Solid Film*, 2012, **520**, 6274.
16 H. Asanuma, K. Shriasuka, T. Takarada, H. Kashida and M. Komiyama, *J. Am. Chem Soc.*, 2003, **125**, 2217.
17 E. Rivera, M. d. P. Carreon-Castro, I. Buendia and G. Cedillo, *Dyes Pigments*, 2006, **68**, 217.
18 R .C. Advincula, E. Fells and M.-k. Park, *Chem. Mater.*, 2001, **13**, 2870.
19 K. K. Karukstis, L. A. Perelman and W. K. Wong, *Langmuir*, 2002, **18**, 10363.
20 M . Mas-Montoya and R. A. J. Janssen, *Adv. Funct. Mater.*, 2017, **27**, 1605779.
21 N. J. Hestand and F. C. Spano, *Chem. Rev.*, 2018, **118**, 7069.
22 R. T. Buwalda, J. M. Jonker, and J. B. F. N. Engberts, *Langmuir*, 1999, **15**, 1083.
23 L. Zhang, X. Liu, W. Rao and J. Li, *Sci. Rep.*, 2016, **6**, 35893.
24 L. Zhang and J. M. Cole, *Appl. Mater. Inter.*, 2014, **6**, 15760.
25 M. Wubs and J. Knoester, *J. Lumin.*, 1998, **76&77**, 359.
26 S. Shekhar, D. Cho, D.-g. Cho, M. Yang, S. Hong, *Nanotechnol.*, 2018, **29**, 205204.
27 M. Yang, D. Cho, J. Kim, N. Shin, S. Shekhar and S. Hong, *Small*, 2018, **14**, 1800885.
28 D. Cho, T. Hwang, D.-g. Cho, B. Park and S. Hong, *Nano Energy*, 2018, **43**, 29.

29 M. D. Irwin, D. B. Buchholz, A. W. Hains, R. P. H. Chang and T. J. Marks, *Proc. Natl. Acad. Sci.*, 2008, **105**, 2783.
30 X.-D. Dang, A. B. Tamayo, J. Seo, C. V. Hoven, B. Walker and T.-Q. Nguyen, *Adv. Funct. Mater.*, 2010, **20**, 3314.
31 D.-C. Coffey, O. G. Reid, D. B. Rodovsky, G. P. Bartholomew, B. Walker and D. S. Ginger, *Nano Lett.*, 2007, **7**, 238.
32 J. L. Luria, N. Hoepker, R. Bruce, A. R. Jacobs, C. Groves and J. A. Marohn, *ACS Nano*, 2012, **11**, 9392.
33 M. Engelson, Modern Spectrum Analyzer Theory and Applications, Artech House, 1984.
34 S. Shekhar, D. Cho, H. Lee, D.-g. Cho and S. Hong, *Nanoscale*, 2016, **8**, 835.
35 H. Asanuma, K. Shirasuka, T. Takarada, H. Kasida and M. Komiyama, *J. Am. Chem. Soc.*, 2003, **125**, 2217.
36 R. T. Narayan and K. D. Veeranna, *J. Appl. Chem.*, 2014, **76**, 762.
37 G. J. Lee, D. Kim and M. Lee, *Appl. Opt.*, 1995, **34**, 138.
38 M.-C Wu, M.-P. Lin, S. W. Chen, P. H. Lee, J.-H. Li and W. -F. Su, *RSC Adv.*, 2014, **4**, 10043.
39 M. S. Masoud and H. H. Hammud, *Spectrochimica Acta A*, 2001, **57**, 977.
40 C. On, E. K. Tanyi, E. Harrison and M. A. Noginov, *Opt. Mater. Exp.*, 2017, **7**, 4286.
41 J. E. Selwyn and J. I. Steinfeld, *J. Phys. Chem.*, 1972, **76**, 762.
42 S. Cook, H. Ohkita, Y. Kim, J. J. Benson-Smith, D. D. C. Bradley and J. R. Durrant, *Chem. Phys. Lett.*, 2007, **445**, 276.
43 O. O. Ogunsolu, J. C. Wang and K. Hanson, *Inorg. Chem.*, 2017, **56**, 11168.
44 G. Zuo, Z. Li, H. Andersson, H. Abdalla, E. Wang and M. Kemerink, *J. Phys. Chem. C*, 2017, **121**, 7767.
45 H. Suzuki and S. Hosino, *J. Appl. Phys.*, 1996, **79**, 8816.
46 H. Kang and V. Subramanian, *Appl. Phys. Lett.*, 2014, **104**, 023301.
47 J. L. Bricks, Y. L. Solminskii, I. D. Panas and A. P. Demchenko, *Methods Appl. Fluoresc.*, 2018, **6**, 012001.
48 M. Kuik, L. J. A. Koster, G. A. H. Wetzelaer and P. W. M. Blom, *Phys. Rev. Lett.*, 2011, **107**, 256805.
49 I. I. Fishchuk, A. K. Kadashchuk, A. Vakhnin, Y. Korosko, H. Bassler, B. Souharce and U. Scherf, *Phys. Rev. B*, 2006, **73**, 115210.
50 C.-M. Li, T. Sjodin and H.-L. Dai, *Phys. Rev. B*, 1997, **56**, 15252.
51 R. H. Bube and H. E. MacDonald, *Phys. Rev.*, 1961, **121**, 473.
52 M. L. Tietze, L. Burtone, M. Riede, B. Lussem and K. Leo, *Phys. Rev. B*, 2012; **86**, 035320.
53 M. L. Tietze, P. Pahner, K. Schmidt, K. Leo and B. Lussem, *Adv. Funct. Mater.*, 2015, **25**, 2701.
54 J. N. Coleman, S. Curran, A. B. Dalton, A. P. Davey, B. Mc Carthy, W. Balu and R. C. Barklie, *Synth. Met.*, 1999, **102**, 1174.
55 M. A. Drobizhev, M. N. Sapozhnikov, I. G. Scheblykin, O. P. Varnavsky, M. V. der Auweraer and A. G. Vitukhnovsky, *Chem. Phys.*, 1996, **211**, 455.
56 A. V. Sorokin, N. V. Pereverzev, I. I. Grankina, S. L. Yefimova, and Y. V. Malyukin, *J. Phys. Chem. C*, 2015, **119**, 27865.
57 A. V. Sorokin, I. Y. Ropakova, S. Wolter, R. Lange, I. Barke, S. Speller, S. L. Yefimova, Y. R. Malyukin and S. Lochbrunner, *J. Phys. Chem. C*, 2019, **123**, 9428.
58 M. Wubs and J. Knoester, *Chem. Phys. Lett.*, 1998, **284**, 63.
59 Y. Lan, B. J. Dringoli, D. A. Valverde-Chavez, C. S. Ponseca Jr., M. Sutton, Y. He, M. G. Kanatzidis and D. G. Cooke, *Sci. Adv.*, 2019, **5**, 5558.
60 R. S. Crandall, *J. Appl. Phys.*, 1983, **54**,7176.
61 Y. S. Lee, T. Gershon, O. Gunawan, T. K. Todorov, T. Gokman, Y. Virgus and S. Guha, *Adv. Energy Mater.*, 2015, **5**, 1401372.
62 Z. Z. Bandic, P. M. Bridger and E. C. Piquette, T. C. McGill, *Appl. Phys. Lett.*, 1998, **73**, 3276.
63 R. Jayaraman and C. G. Sodini, *IEEE Trans. Electron Devices*, 1989, **36**, 1773.
64 Z. Celik-Butler, and T. Y. Hsiang, *IEEE Trans. Electron Devices*, 1988, **35**, 1651.
65 J. Bisquert, F. Fabregat-Santiago, I. Mora-Sero, G. Garcia-Belmonte and S. Gimenez, *J. Phys. Chem. C*, 2009, **113**, 17278.
66 D. F. Swinehart, *J. Chem. Edu.*, 1962, **39**, 333.

View Article Online
DOI: 10.1039/D0TA07328H

View Article Online
DOI: 10.1039/D0TA07328H

TOC

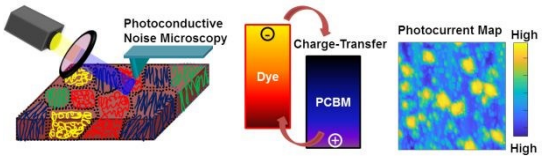

The dye film shows the formation of various aggregates which have the wavelength–dependent solar cell performances.

Electronic Supplementary Information

PAPER

Nanoscale Mapping of Wavelength–Selective Photovoltaic Responses in H– and J–Aggregates of Azo Dye–based Solar Cell Films

Received 27th July 2020,
Accepted 00th January 20xx

DOI: 10.1039/x0xx00000x

Shashank Shekhar,[a] Inkyoung Park,[a] Jeongsu Kim,[a] Myungjae Yang,[a] Duckhyung Cho[a] and Seunghun Hong *[a]

.

[a] *Department of Physics and Astronomy, and Institute of Applied Physics, Seoul National University, Seoul, 08826, Korea. E-mail:seunghun@snu.ac.kr*

† Footnotes relating to the title and/or authors should appear here.
Electronic Supplementary Information (ESI) available: [Current and noise maps of dye solar cell films]. See DOI: 10.1039/x0xx00000x

Current Map

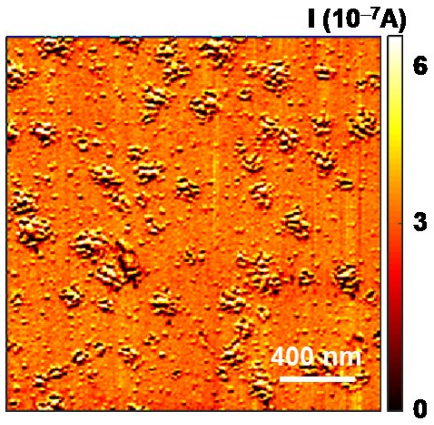

Fig. S1 Current map of dye solar cell film at the applied bias of 0.1 V under the dark condition.

Change in trap density dependence on initial trap density

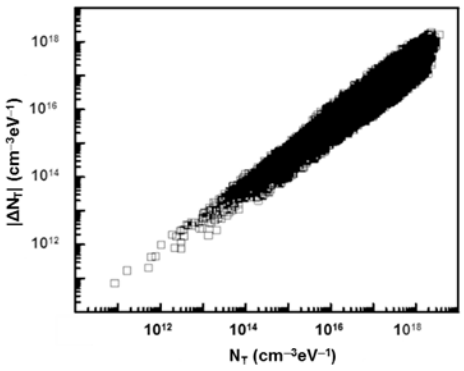

Fig. S3 Scatter plot showing the dependence of trap density change by illumination on the trap density under dark conditions.

Noise Map

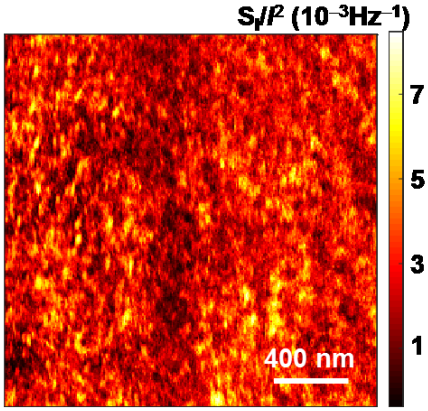

Fig. S2 Normalized noise PSD (S_I/I^2) map of the dye solar cell film under the dark condition at the applied bias of 0.1 V.